Structural Engineering and Mechanics, *Vol. 68, No. 3 (2018) 359-368*
DOI: https://doi.org/10.12989/sem.2018.68.3.359

Dynamic instability response in nanocomposite pipes conveying pulsating ferrofluid flow considering structural damping effects

Hemat Ali Esmaeili, Mehran Khaki* and Morteza Abbasi

Department of Mechanical Engineering, Sari Branch, Islamic Azad University, Sari, Iran

(Received August 3, 2018, Revised September 13, 2018, Accepted September 18, 2018)

Abstract. This paper deals with the dynamic stability of nanocomposite pipes conveying pulsating ferrofluid. The pipe is reinforced by carbon nanotubes (CNTs) where the agglomeration of CNTs are considered based on Mori-Tanaka model. Due to the existence of CNTs and ferrofluid flow, the structure and fluid are subjected to axial magnetic field. Based on Navier-Stokes equation and considering the body forced induced by magnetic field, the external force of fluid to the pipe is derived. For mathematical modeling of the pipe, the first order shear deformation theory (FSDT) is used where the energy method and Hamilton's principle are used for obtaining the motion equations. Using harmonic differential quadrature method (HDQM) and Bolotin's method, the motion equations are solved for calculating the excitation frequency and dynamic instability region (DIR) of the structure. The influences of different parameters such as volume fraction and agglomeration of CNTs, magnetic field, structural damping, viscoelastic medium, fluid velocity and boundary conditions are shown on the DIR of the structure. Results show that with considering agglomeration of CNTs, the DIR shifts to the lower excitation frequencies. In addition, the DIR of the structure will be happened at higher excitation frequencies with increasing the magnetic field.

Keywords: dynamic stability; pulsating ferrofluid flow; CNTs; agglomeration; magnetic field

1. Introduction

As it is known, ferrofluid has magnetic properties and it can be strongly magnetized in the presence of a magnetic field. Ferrofluid is containing the ferromagnetic nanoparticles and can be used in electronic devices, semi-active dampers in mechanical and aerospace engineerings, loudspeakers, medical applications, heat transfer and Energy harvesting (Sanada 2018).

Dynamic analysis of different structures in contact with fluid has been reported by some researchers. Temperature-dependent nonlinear vibration and instability of embedded functionally graded (FG) pipes conveying viscous fluid-nanoparticle mixture were studied by Raminnea *et al.* (2016). Vibration analysis of fluid conveying microbeams under non-ideal boundary conditions (BCs) was performed by Atcı and Bağdatlı (2017). Shokravi and jalili (2017) presented nonlinear vibration and instability of cylindrical shell conveying fluid-nanoparticles mixture flow. Vakili Tahami *et al.* (2017) studied Dynamic response of functionally graded Carbon nanotubes (FG-CNT) reinforced pipes conveying viscous fluid under accelerated moving load. Ghaitani amd Majidian (2017) addressed vibration and instability of embedded functionally graded (FG)-carbon nanotubes (CNTs)-reinforced pipes conveying viscous fluid. Vibration and stability of concrete pipes reinforced with carbon nanotubes (CNTs) conveying fluid were presented by Zamani Nouri (2017). Ghayesh and Farokhi (2017) analyzed the coupled fluid-structure viscoelastic dynamical characteristics of a fluid-conveying viscoelastic microtube resting on a nonlinear elastic bed subject to large rotations. The free vibration analysis of fluid conveying Timoshenko pipeline with different boundary conditions using Differential Transform Method (DTM) and Adomian Decomposition Method (ADM) was investigated by Bozyigit *et al.* (2017). Zamani Nouri (2018) studied stability analysis of concrete pipes mixed with nanoparticles conveying fluid.

Dynamic response of structure reinforced by CNTs considering agglomeration effect is one of the interest topic among the researchers. By considering the agglomeration effect of single-walled carbon nanotubes, free vibration characteristics of functionally graded (FG) nanocomposite sandwich beams resting on Pasternak foundation were presented by Kamarian *et al.* (2015). Duc *et al.* (2015) investigated on the nonlinear dynamic response and vibration of the imperfect laminated three-phase polymer nanocomposite panel resting on elastic foundations and subjected to hydrodynamic loads. Tornabene *et al.* (2016) studied the effect of Carbon Nanotube (CNT) agglomeration on the free vibrations of laminated composite doubly-curved shells and panels reinforced by CNTs. A free vibration analysis of Carbon Nanotube-Reinforced Composite (CNTRC) conical shells was performed by Kamarian *et al.* (2016) considering the agglomeration effect of Carbon Nanotubes (CNTs). The static response of composite plates and shells reinforced by agglomerated nanoparticles made of Carbon Nanotubes (CNTs) was investigated by Tornabene *et al.* (2017). Duc *et al.* (2017) analyzed a new approach-using analytical solution to investigate nonlinear dynamic response and

*Corresponding author, Ph.D.
E-mail: mehran.khaki@gmail.com

ISSN: 1225-4568 (Print), 1598-6217 (Online)

vibration of imperfect functionally graded carbon nanotube reinforced composite (FG-CNTRC) double curved shallow shells. Thu *et al.* (2017) studied an analytical approach to investigate the non-linear dynamic response and vibration of an imperfect three-phase laminated nanocomposite cylindrical panel resting on elastic foundations in thermal environments. Based on the strain gradient theory (SGT), vibration analysis of an embedded micro cylindrical shell reinforced with agglomerated carbon nanotubes (CNTs) was investigated by Tohidi *et al.* (2017). Shokravi (2017) studied nonlinear vibration of embedded nanocomposite concrete is investigated based on Timoshenko beam model. García-Macías and Castro-Triguero (2018) comprised general axisymmetric orientation distributions of fillers, both planar sinusoidal and helical wavy fillers, as well as different agglomeration schemes by means of a two-parameter agglomeration model. Duc *et al.* (2018) presented the first analytical approach to investigate the nonlinear dynamic response and vibration of imperfect rectangular nanocompsite multilayer organic solar cell subjected to mechanical loads using the classical plate theory. Cong and Duc (2018) presented an analytical approach to investigate the nonlinear dynamic response and vibration of functionally graded multilayer nanocomposite plates reinforced with a low content of graphene platelets (GPLs) using first-order shear deformation theory and a stress function with full motion equations (not using Volmir's assumptions).

To the best of our knowledge, no investigation has been performed on the dynamic stability of pipes conveying ferrofluid. In this paper, the dynamic stability of pipes reinforced by agglomerated CNTs conveying ferrofluid is presented. The structural damping of the pipes is considered and the surrounding viscoelastic medium is modeled by visco-Pasternak model. Based on FSDT, energy method and Hamilton's principle, the motion equations are derived. Utilizing HDQM and Boltin's method, the DIR of the structure is obtained and the effects of volume fraction and agglomeration of CNTs, magnetic field, structural damping, viscoelastic medium, fluid velocity and boundary conditions are shown on the DIR of the structure.

2. Formulation

Fig. 1 shows a pipe reinforced by agglomerated CNTs conveying ferrofluid subjected to axial magnetic field. The pipe has length L, average radius R and thickness h. The surrounding viscoelastic medium is simulated with spring, shear and damper elements.

Based on FSDT, the displacement fields can be written as (Reddy 2002)

$$u_1(x,\theta,z,t)=u(x,\theta,t)+z\psi_x(x,\theta,t), \tag{1}$$

$$u_2(x,\theta,z,t)=v(x,\theta,t)+z\psi_\theta(x,\theta,t), \tag{2}$$

$$u_3(x,\theta,z,t)=w(x,\theta,t), \tag{3}$$

where u, v and w are mid-plane displacements in the axial, circumferential and lateral directions, respectively; $\psi_x(x,\theta,t)$ and $\psi_\theta(x,\theta,t)$ are the rotations of the normal to the mid-plane about x- and θ-directions, respectively. However, the nonlinear strain-displacement relations can be derived as

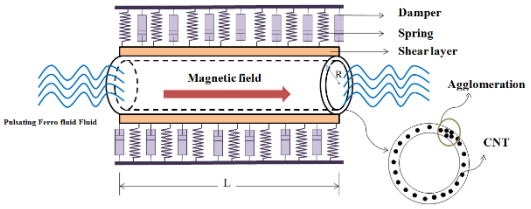

Fig. 1 Schematic of pipe reinforced by agglomerated CNTs conveying ferrofluid subjected to axial magnetic field

$$\varepsilon_{xx}=\frac{\partial u}{\partial x}+\frac{1}{2}\left(\frac{\partial w}{\partial x}\right)^2+z\frac{\partial \psi_x}{\partial x}, \tag{4}$$

$$\varepsilon_{\theta\theta}=\frac{\partial v}{R\partial\theta}+\frac{w}{R}+\frac{1}{2}\left(\frac{\partial w}{R\partial\theta}\right)^2+z\frac{\partial \psi_\theta}{R\partial\theta}, \tag{5}$$

$$\gamma_{\theta z}=\frac{\partial w}{R\partial\theta}-\frac{v}{R}+\psi_\theta, \tag{6}$$

$$\gamma_{xz}=\frac{\partial w}{\partial x}+\psi_x, \tag{7}$$

$$\gamma_{x\theta}=\frac{\partial v}{\partial x}+\frac{\partial u}{R\partial\theta}+\frac{\partial w}{\partial x}\frac{\partial w}{R\partial\theta}+z\left(\frac{\partial \psi_x}{R\partial\theta}+\frac{\partial \psi_\theta}{\partial x}\right). \tag{8}$$

3. Mori-Tanaka model

Based on Mori-Tanaka model and considering agglomeration of CNTs, the effective Young's modulus E and Poisson's ratio v of the composite material are given by (Mori and Tanaka 1973)

$$E=\frac{9KG}{3K+G}, \tag{9}$$

$$\upsilon=\frac{3K-2G}{6K+2G}. \tag{10}$$

where the effective bulk modulus K and shear modulus G may be written as below

$$K=K_{out}\left[1+\frac{\xi\left(\frac{K_{in}}{K_{out}}-1\right)}{1+\alpha(1-\xi)\left(\frac{K_{in}}{K_{out}}-1\right)}\right], \tag{11}$$

$$G = G_{out}\left[1+\frac{\xi\left(\frac{G_{in}}{G_{out}}-1\right)}{1+\beta\left(1-\xi\right)\left(\frac{G_{in}}{G_{out}}-1\right)}\right], \tag{12}$$

where ξ and ζ are agglomeration parameters; K_{in} and K_{out} are the effective bulk modulus of the inclusion and the matrix outside the inclusion, respectively. Also, G_{in} and G_{out} are the effective shear modulus of the inclusion and the matrix outside the inclusion, respectively and are given as follows

$$K_{in} = K_m + \frac{\left(\delta_r - 3K_m\chi_r\right)C_r\zeta}{3\left(\xi - C_r\zeta + C_r\zeta\chi_r\right)}, \tag{13}$$

$$K_{out} = K_m + \frac{C_r\left(\delta_r - 3K_m\chi_r\right)\left(1-\zeta\right)}{3\left[1-\xi-C_r\left(1-\zeta\right)+C_r\chi_r\left(1-\zeta\right)\right]}, \tag{14}$$

$$G_{in} = G_m + \frac{\left(\eta_r - 3G_m\beta_r\right)C_r\zeta}{2\left(\xi - C_r\zeta + C_r\zeta\beta_r\right)}, \tag{15}$$

$$G_{out} = G_m + \frac{C_r\left(\eta_r - 3G_m\beta_r\right)\left(1-\zeta\right)}{2\left[1-\xi-C_r\left(1-\zeta\right)+C_r\beta_r\left(1-\zeta\right)\right]}, \tag{16}$$

where C_r is volume percent of CNTs; $\chi_r, \beta_r, \delta_r$ and η_r can be obtained as

$$\chi_r = \frac{3\left(K_m + G_m\right) + k_r - l_r}{3\left(k_r + G_m\right)}, \tag{17}$$

$$\beta_r = \frac{1}{5}\left\{\begin{array}{l}\dfrac{4G_m + 2k_r + l_r}{3\left(k_r + G_m\right)} + \dfrac{4G_m}{\left(p_r + G_m\right)} \\ + \dfrac{2\left[G_m\left(3K_m + G_m\right) + G_m\left(3K_m + 7G_m\right)\right]}{G_m\left(3K_m + G_m\right) + m_r\left(3K_m + 7G_m\right)}\end{array}\right\}, \tag{18}$$

$$\delta_r = \frac{1}{3}\left[n_r + 2l_r + \frac{\left(2k_r - l_r\right)\left(3K_m + 2G_m - l_r\right)}{k_r + G_m}\right], \tag{19}$$

$$\eta_r = \frac{1}{5}\left[\begin{array}{l}\dfrac{2}{3}\left(n_r - l_r\right) + \dfrac{8G_m m_r\left(3K_m + 4G_m\right)}{3K_m\left(m_r + G_m\right) + G_m\left(7m_r + G_m\right)} \\ + \dfrac{2\left(k_r - l_r\right)\left(2G_m + l_r\right)}{3\left(k_r + G_m\right)} + \dfrac{4G_m p_r}{\left(p_r + G_m\right)}\end{array}\right], \tag{20}$$

where k_r, l_r, n_r, p_r and m_r are Hill's elastic moduli; K_m and G_m are the bulk and shear moduli of the matrix phase which are defined as below

$$K_m = \frac{E_m}{3\left(1-2\upsilon_m\right)}, \tag{21}$$

$$G_m = \frac{E_m}{2\left(1+\upsilon_m\right)}. \tag{22}$$

Moreover, α and β in Eqs. (11) and (12) are given as follows

$$\alpha = \frac{\left(1+\upsilon_{out}\right)}{3\left(1-\upsilon_{out}\right)}, \tag{23}$$

$$\beta = \frac{\left(1+\upsilon_{out}\right)}{3\left(1-\upsilon_{out}\right)}, \tag{24}$$

$$\upsilon_{out} = \frac{3K_{out} - 2G_{out}}{6K_{out} + 2G_{out}}. \tag{25}$$

Based on Kelvin-Voigt theory, the Young's modulus can be written as (Lakes 2209)

$$E \to E\left(1 + g\frac{\partial}{\partial t}\right) \tag{26}$$

where g is the structural damping parameter.

3. Motion equations

3.1 Potential energy

The potential energy of the structure is

$$\begin{aligned} U = 0.5\int \Bigg(& N_{xx}\left(\frac{\partial u}{\partial x} + \frac{1}{2}\left(\frac{\partial w}{\partial x}\right)^2\right) + N_{\theta\theta}\left(\frac{\partial v}{R\partial\theta} + \frac{w}{R} + \frac{1}{2}\left(\frac{\partial w}{R\partial\theta}\right)^2\right) \\ & + Q_\theta\left(\frac{\partial w}{R\partial\theta} - \frac{v}{R} + \psi_\theta\right) + Q_x\left(\frac{\partial w}{\partial x} + \psi_x\right) + N_{x\theta}\left(\frac{\partial v}{\partial x} + \frac{\partial u}{R\partial\theta} + \frac{\partial w}{\partial x}\frac{\partial w}{R\partial\theta}\right) \\ & + M_{xx}\frac{\partial\psi_x}{\partial x} + M_{\theta\theta}\frac{\partial\psi_\theta}{R\partial\theta} + M_{x\theta}\left(\frac{\partial\psi_x}{R\partial\theta} + \frac{\partial\psi_\theta}{\partial x}\right)\Bigg) dA, \end{aligned} \tag{27}$$

where the resultant force and moments may be calculated as

$$\begin{bmatrix} N_{xx} \\ N_{\theta\theta} \\ N_{x\theta} \end{bmatrix} = \int_{-h/2}^{h/2}\begin{bmatrix} \sigma_{xx} \\ \sigma_{\theta\theta} \\ \tau_{x\theta} \end{bmatrix} dz, \tag{28}$$

$$\begin{bmatrix} M_{xx} \\ M_{\theta\theta} \\ M_{x\theta} \end{bmatrix} = \int_{-h/2}^{h/2}\begin{bmatrix} \sigma_{xx} \\ \sigma_{\theta\theta} \\ \sigma_{x\theta} \end{bmatrix} z dz, \tag{29}$$

$$\begin{bmatrix} Q_x \\ Q_\theta \end{bmatrix} = \int_{-h/2}^{h/2}\begin{bmatrix} k'\tau_{xz} \\ k'\tau_{z\theta} \end{bmatrix} dz, \tag{30}$$

where k' is shear correction factor. Using Eqs. (4)-(9), the resultant force and moments can be written as shown in Appendix A.

3.2 Kinetic energy

The kinetic energy of the structure may be expressed as

$$K = 0.5\int \left[I_0\left(\left(\frac{\partial u}{\partial t}\right)^2+\left(\frac{\partial v}{\partial t}\right)^2+\left(\frac{\partial w}{\partial t}\right)^2\right) +2I_1\left(\frac{\partial u}{\partial t}\frac{\partial \psi_x}{\partial t}+\frac{\partial v}{\partial t}\frac{\partial \psi_\theta}{\partial t}\right)+I_2\left(\left(\frac{\partial \psi_x}{\partial t}\right)^2+\left(\frac{\partial \psi_\theta}{\partial t}\right)^2\right)\right]dA. \tag{31}$$

where ρ is the density of nanocomposite pipe; the moment of inertia can be written as

$$\begin{Bmatrix} I_0 \\ I_1 \\ I_2 \end{Bmatrix} = \int_{-h/2}^{h/2} \begin{bmatrix} \rho \\ \rho z \\ \rho z^2 \end{bmatrix} dz, \tag{32}$$

3.3 Work of viscoelastic medium

The work of surrounded viscoelastic medium is

$$W_v = \int_A \left(-k_w w + k_g \nabla^2 w - c_v \left[\frac{\partial w}{\partial t} \right] \right) w dA, \tag{33}$$

where k_w, k_g and c_v are spring, shear and damping modulus, respectively.

3.4 Work of ferrofluid fluid

In order to calculate the work down by fluid, the well-down Navies-Stokes equation is used as follows (Wang and Ni 2009)

$$\rho_f \frac{D\mathrm{V}}{Dt} = -\nabla \mathrm{P} + \mu \nabla^2 \mathrm{V} + \mathrm{F}_{body\ force}, \tag{34}$$

where V=(v_r, v_θ, v_x) is the flow velocity in a cylindrical coordinate system, ρ_f, P and μ are fluid density, static pressure and fluid viscosity, respectively. In the Navies-Stokes equation, $\frac{D}{Dt}$ can be defined as follows considering axial fluid velocity

$$\frac{D}{Dt} = \frac{\partial}{\partial t} + v_x \frac{\partial}{\partial x}. \tag{35}$$

At the point of contact between the inside tube and the internal fluid, their respective velocities and accelerations in the direction of flexural displacement become equal. These relationships thus can be written as

$$v_r = \frac{\partial w}{\partial t}. \tag{36}$$

In Eq. (34), $\mathrm{F}_{body\ force}$ is the body force which is due to the axial magnetic field in this paper as follows

$$\vec{F} = \vec{J} \times \vec{B} \tag{37}$$

where $\vec{J}$ is electric current density and magnetic field inside the ferrofluid can be approximated with $\vec{B}$ along the x direction. According to Ohm's law, $\vec{J}$ can be obtained (Qian and Bau 2005, 2009)

$$\vec{J} = \sigma\left(V \times \vec{B}\right) \tag{38}$$

where σ and V are electric conductivity solution and fluid velocity field. $\vec{B}$ is magnetic flux density and the SI unit of magnetic flux density is the Tesla (T). The intensity of the magnetic flux density, $\vec{B}$, is affected by the intensity of the magnetic field, $\vec{H}$. The relationship between magnetic field strength and magnetic flux density is

$$\vec{B} = \mu \times \vec{H} \tag{39}$$

where μ is the magnetic permeability of the substance.

The work down by fluid can be calculated as follows

$$W_f = \int_0^L \int_A \frac{\partial P}{\partial z} dA\, dx = \int_0^L \int_A (\mu_f \frac{\partial^2}{\partial x^2}(\frac{\partial w}{\partial t} + V_f \frac{\partial w}{\partial x}) +\sigma(B_x^2)(\frac{\partial w}{\partial t} + V_f \frac{\partial w}{\partial x}) - \rho_f (\frac{\partial}{\partial t} + V_f \frac{\partial}{\partial x})(\frac{\partial w}{\partial t} + V_f \frac{\partial w}{\partial x}))dA\, dx \tag{40}$$

The pulsating internal flow is assumed harmonically as follows

$$v_x = V_0(1 + \beta \cos(\omega t)), \tag{41}$$

where V_0, β and ω are the mean flow velocity, the harmonic amplitude and pulsation frequency, respectively.

3.5 Work of magnetic field

The work down by fluid can be calculated as follows (Kiani 2014)

$$W_m = \int_0^L \int_A \left(\eta h H_x^2 \left(\frac{\partial^2 w}{\partial x^2} - \frac{\partial^2 w}{R^2 \partial \theta^2} \right) \right) w\, dA. \tag{42}$$

where η is the magnetic permeability and H_x is the magnetic field.

3.6 Hamilton's principle

Using Hamilton's principle, the variational form of the equations of motion can be expressed by

$$\delta \int_0^t \Pi\, dt = \delta \int_0^t \left[K - \left(U - \left\{ W_V + W_F + W_M \right\} \right) \right] dt = 0. \tag{43}$$

By applying the Hamilton's principle and sorting of mechanical displacement, five governing equations are obtained as follows

$$\delta u: \quad \frac{\partial N_{xx}}{\partial x} + \frac{\partial N_{x\theta}}{R \partial \theta} = I_0 \frac{\partial^2 u}{\partial t^2} + I_1 \frac{\partial^2 \psi_x}{\partial t^2}, \tag{44}$$

$$\delta v: \quad \frac{\partial N_{x\theta}}{\partial x}+\frac{\partial N_{\theta\theta}}{R\partial\theta}+\frac{Q_\theta}{R}=I_0\frac{\partial^2 v}{\partial t^2}+I_1\frac{\partial^2\psi_\theta}{\partial t^2}, \tag{45}$$

$$\begin{aligned}\delta w: \quad & \frac{\partial Q_x}{\partial x}+\frac{\partial Q_\theta}{R\partial\theta}-k_w w+k_g\nabla^2 w-c_v\dot{w}\\ & +\mu_f\frac{\partial^2}{\partial x^2}\left(\frac{\partial w}{\partial t}+v_x\frac{\partial w}{\partial x}\right)+\sigma H_x^2\left(\frac{\partial w}{\partial t}+v_x\frac{\partial w}{\partial x}\right)\\ & -\rho_f\left(\frac{\partial}{\partial t}+V_f\frac{\partial}{\partial x}\right)\left(\frac{\partial w}{\partial t}+v_x\frac{\partial w}{\partial x}\right)\\ & +\eta h H_x^2\left(\frac{\partial^2 w}{\partial x^2}-\frac{\partial^2 w}{R^2\partial\theta^2}\right)=I_0\frac{\partial^2 w}{\partial t^2},\end{aligned} \tag{46}$$

$$\delta\psi_x: \quad \frac{\partial M_{xx}}{\partial x}+\frac{\partial M_{x\theta}}{R\partial\theta}-Q_x=I_1\frac{\partial^2 u}{\partial t^2}+I_2\frac{\partial^2\psi_x}{\partial t^2}, \tag{47}$$

$$\delta\psi_\theta: \quad \frac{\partial M_{x\theta}}{\partial x}+\frac{\partial M_{\theta\theta}}{R\partial\theta}-Q_\theta=I_1\frac{\partial^2 v}{\partial t^2}+I_2\frac{\partial^2\psi_\theta}{\partial t^2}, \tag{48}$$

Substituting Eqs. (A1)-(A7) into Eqs. (44)-(48) yields the motion equations (Appendix B)

In this paper, three types of boundary conditions are considered as

• Simple-Simple (SS)

$$x=0,L\Rightarrow u=v=w=\phi_\theta=M_x=0, \tag{49}$$

• Clamped- Clamped (CC)

$$x=0,L\Rightarrow u=v=w=\phi_x=\phi_\theta=0, \tag{50}$$

• Clamped- Simple (CS)

$$\begin{aligned}&x=0\Rightarrow u=v=w=\phi_x=\phi_\theta=0,\\ &x=L\Rightarrow u=v=w=\phi_x=M_x=0.\end{aligned} \tag{51}$$

4. Solution procedures

Based on HDQM, the differential equations can be changed to algebraic equations as follows (Civalek 2004, Rehab *et al.* 2018, Henderson *et al.* 2018)

$$\frac{d^n F(x_i,\theta_j)}{dx^n}=\sum_{k=1}^{N_x}A_{ik}^{(n)}F(x_k,\theta_j) \qquad n=1,...,N_x-1, \tag{52}$$

$$\frac{d^m F(x_i,\theta_j)}{d\theta^m}=\sum_{l=1}^{N_\theta}B_{jl}^{(m)}F(x_i,\theta_l) \qquad m=1,...,N_\theta-1, \tag{53}$$

$$\frac{d^{n+m}F(x_i,\theta_j)}{dx^n d\theta^m}=\sum_{k=1}^{N_x}\sum_{l=1}^{N_\theta}A_{ik}^{(n)}B_{jl}^{(m)}F(x_k,\theta_l), \tag{54}$$

where $A_{ik}^{(n)}$ and $B_{jl}^{(m)}$ are the weighting coefficients and N_x and N_θ are grid points which can be calculated by Chebyshev polynomials. Applying HDQM and using Eqs. (52)-(54) to motion equations and boundary conditions results governing equations can be expressed as

$$\begin{aligned}&\left(\begin{aligned}&[K]+\left(u_f\left[1+\alpha\cos(\omega t)\right]\right)[K]^f\\ &+\left(u_f\left[1+\alpha\cos(\omega t)\right]\right)^2[K]^{ff}\end{aligned}\right)\{d\}\\ &+\left([C]+\left(u_f\left[1+\alpha\cos(\omega t)\right]\right)[C]^f\right)\{\dot{d}\}\\ &+[M]\{\ddot{d}\}=0,\end{aligned} \tag{55}$$

where $[K]^f$, $[K]^{ff}$ and $[C]^f$ are stiffness matrix coefficients, damping coefficient matrix coefficients of pulsating fluid; $[M]$ is matrices of mass; d_b and d_d are related to the boundary and domain points, respectively. To solve the Eq. (55), the Bolotin's method is used. In this way displacement vector $\{d\}$ be considered as follows (Patel 2006)

$$\{d\}=\sum_{k=1,3,...}^{\infty}\left[\{a\}_k\sin\frac{k\omega t}{2}+\{b\}_k\cos\frac{k\omega t}{2}\right], \tag{56}$$

According to the published works in the field of dynamic instability, the first dynamic instability region is the most important with respect to other regions (Patel 2006). Finally, by substituting the Eq. (56) in Eq. (55) and separate *sinus* and *cosinus* coefficients, we have

$$\begin{aligned}&\left|\left([K]+\left(1\pm\frac{\alpha}{2}\right)[K]^f+\left(1\pm\alpha+\frac{\alpha^2}{2}\right)[K]^{ff}\right)\right.\\ &\left.+\left(\pm[C]\frac{\omega^2}{2}+\left(\frac{\alpha\omega}{4}\pm\frac{\omega}{2}\right)[C]^f\right)-[M]\frac{\omega^2}{4}\right|=0.\end{aligned} \tag{57}$$

Using eigenvalue problem and direct iterative method, Eq. (57) can be solved to obtain the variation of ω with respect to α as DIR of system can be obtained.

5. Numerical results

For parametric study, a polymer pipe made from polyethylene (PE) with the Young's modulus of E_m=0.3 *Gpa*, Poisson's ration of v_m=0.3, length to thickness ratio of L/h=20 and thickness to radius ratio of h/R=0.03 is considered. The pipe is reinforced by agglomerated CNTs with the Hills elastic modulus reported in (Mori and Tanaka 1973). The inside fluid is water with AL_3O_4 magnetic nanoparticles with the density of ρ_f=1000 Kg/m^3 and viscosity of μ=8.9×10^{-4} *Pa*.s.

5.1 Convergence of HDQM

In order to show the accuracy of the proposed numerical method, Fig. 2 is plotted. In this figure, DIR of the structure is plotted for different values of grid point numbers. It can be seen that with increasing the grid point numbers, the DIR shifts to left and the results start to converge at N=17.

5.2 Validation

In order to validate the present results, the CNTs as

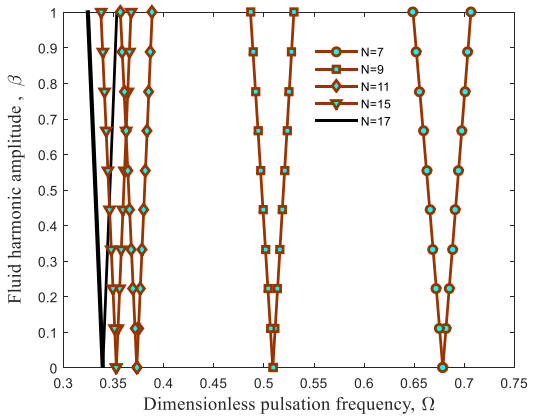

Fig. 2 Convergence and accuracy of HDQM

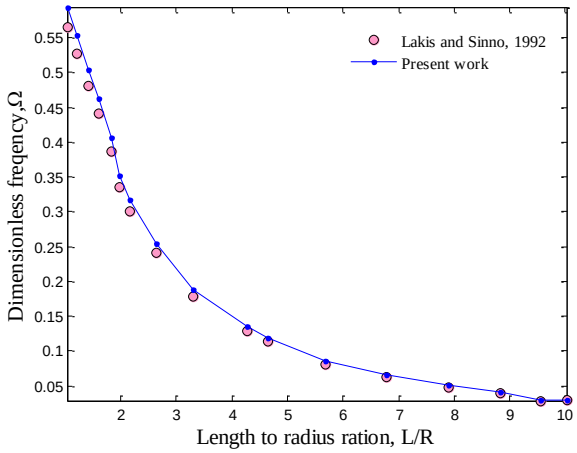

Fig. 3 Validation of present work with (Lakis and Sinno, 1992)

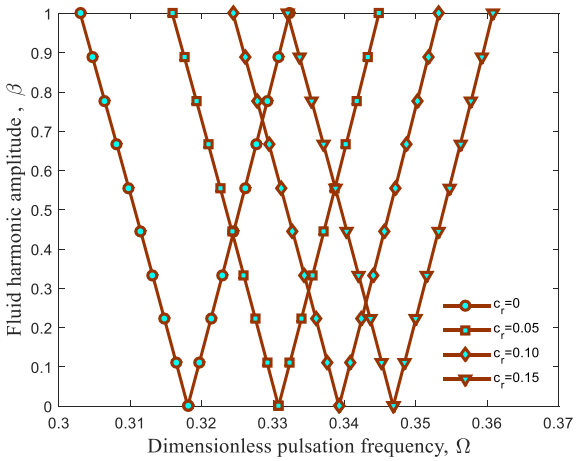

Fig. 4 The effects of CNTs volume percent on the DIR of the structure

reinforcement of the pipe, ferrofluid, structural damping and viscoelastic medium are neglected. However, vibration of a pipe with thickness to radius ratio of h/R=0.02 is studied. Fig. 3 shows the dimensionless frequency ($\Omega = \omega R[\rho_m(1-\upsilon_m{}^2)]^{0.5}$) of the pipe against length to radius ratio. It can be seen that the present results are in a good agreement with (Lakis and Sinno 1992).

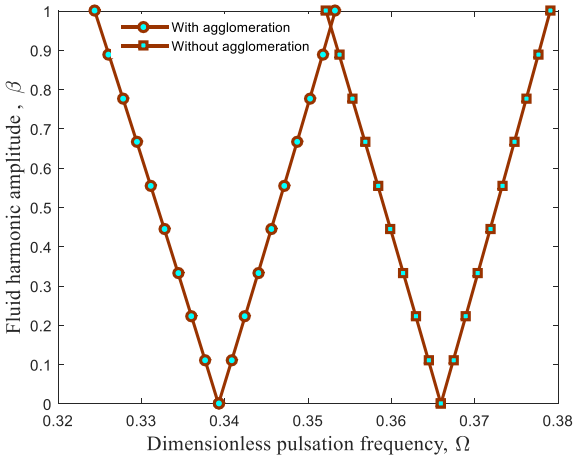

Fig. 5 The effects of CNTs agglomeration on the DIR of the structure

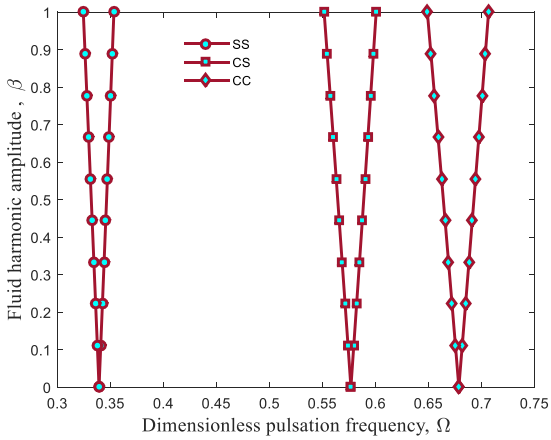

Fig. 6 The effects of boundary conditions on the DIR of the structure

5.3 Parametric study

Fig. 4 shows the effects of CNTs volume fraction on the dimensionless excitation frequency with respect to fluid harmonic amplitude. The regions inside and outside the boundary curves correspond to unstable (parametric resonance) and stable regions, respectively. As can be seen, with increasing the CNTs volume fraction, the DIR shifts to higher frequencies. In other words, increasing the CNTs volume fraction leads to higher resonance frequency which is due to increase in the stiffness of structure.

Depicted in Fig. 5 is the effect of CNTs agglomeration on the dimensionless excitation frequency versus fluid harmonic amplitude. As can be seen, considering agglomeration of CNTs leads to lower excitation frequencies. In other words, with considering agglomeration of CNTs, the DIR will occur at lower excitation frequencies. It can, therefore, be concluded that the agglomeration reduces the stiffness of the structure.

The effect of different boundary conditions is presented in Fig. 6 on the dimensionless excitation frequency versus fluid harmonic amplitude. It can be found that the CC boundary condition yields to higher resonance frequency. In other words, comparing the assumed boundary conditions,

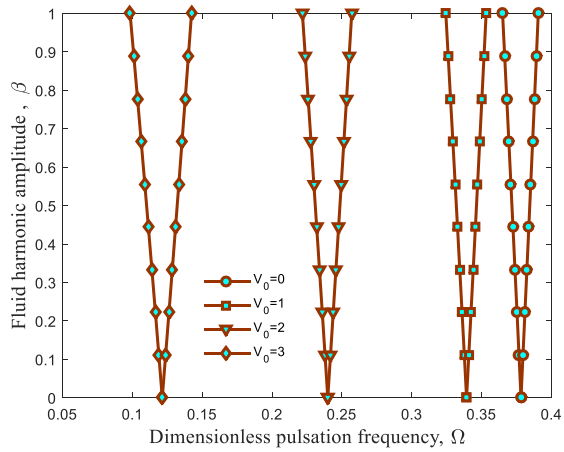

Fig. 7 The effects of dimensionless flow velocity on the DIR of the structure

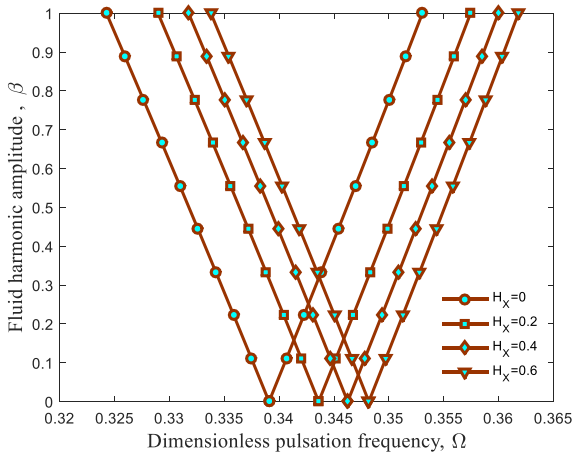

Fig. 8 The effects of axial magnetic field on the DIR of the structure

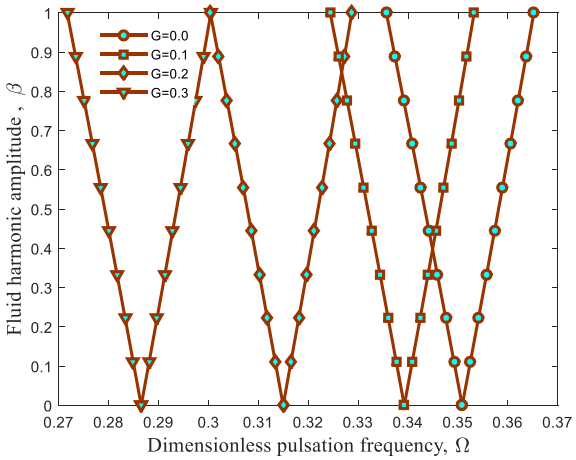

Fig. 9 The effects of structural damping on the DIR of the structure

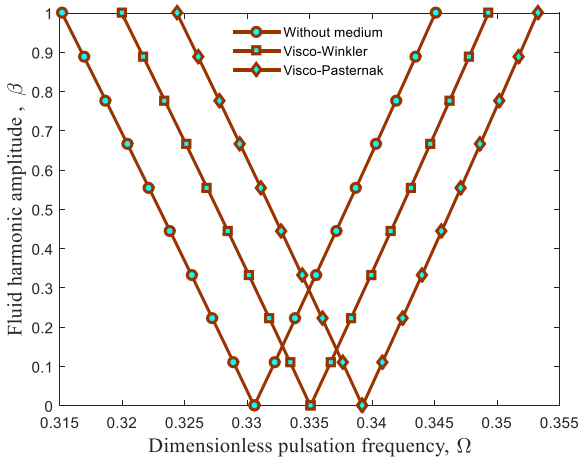

Fig. 10 The effects of surrounding viscoelastic foundation on the DIR of the structure

the DIR of structure moves to right for the case of pipe with CC boundary conditions.

Fig. 7 illustrates the effect of dimensionless flow velocity ($V_0 = v_0[\rho_m / E_m]^{0.5}$) on the DIR of the structure. As can be seen, with increasing fluid velocity, the DIR occurs in lower pulsation frequencies. In addition, the greater fluid velocity leads to large instability zone and low pulsation frequency.

Fig. 8 shows the effect of axial magnetic field intensity on the variations of the dimensionless pulsation frequency versus the fluid pulsation amplitude. As can be seen, with increasing the magnetic field, the DIR shifts to higher excitation frequencies. It is because with increasing the magnetic field, the stiffness of the structure improves.

Fig. 9 demonstrates the DIR for different structural damping constant. As can be seen, the DIR and frequency of viscoelastic pipe is lower than those of non-visco structure (i.e., G=0). This remarkable difference shows that considering the nature of pipe as viscoelastic can yield the accurate results with respect to non-visco micro plate.

The effect of different viscoelastic mediums is demonstrated in Fig. 10 for three cases which are without viscoelastic medium, visco-Winkler medium and visco-Pasternak medium. It can be seen that considering viscoelastic medium increases the excitation frequency of structure and DIR shifts to higher frequencies. It is due to the fact that considering viscoelastic medium leads to stiffer structure. Furthermore, the excitation frequency which leads to DIR for the case of visco-Pasternak medium is higher than the visco-Winkler medium. It is because in the visco-Pasternak medium indeed the normal loads, the shear forces are considered.

6. Conclusions

In this paper, dynamic stability of pipes reinforced by agglomerate CNTs conveying ferrofluid was presented. The structural damping effect was considered and the structure was subjected to axial magnetic field. The surrounding viscoelastic medium was modeled by visco-Pasternak foundation. Based on FSDT, energy method and Hamilton's principle, the motion equations were derived. Using HDQM and Bolotin's method, the DIR of the structure was obtained and the influences of different parameters such as volume fraction and agglomeration of CNTs, magnetic field,

structural damping, viscoelastic medium, fluid velocity and boundary conditions are shown on the DIR of the structure. The most important conclusions of this paper can be enumerated as follows:

• With increasing the CNTs volume fraction, the DIR shifts to higher frequencies.

• With considering agglomeration of CNTs, the DIR will be happened at lower excitation frequencies.

• With increasing fluid velocity, the DIR occurs in lower pulsation frequencies.

• It can be found that the CC boundary condition yields to higher resonance frequency.

• With increasing the magnetic field, the DIR shifts to higher excitation frequencies.

• The DIR and frequency of viscoelastic pipe is lower than those of non-visco structure (i.e., G=0).

References

Atcı, D. and Bağdatlı, S.M. (2017), "Free vibrations of fluid conveying microbeams under non-ideal boundary conditions", *Steel Compos. Struct.*, **24**(2), 141-149.

Bozyigit, B., Yesilce, Y. and Catal, S. (2017), "Differential transform method and Adomian decomposition method for free vibration analysis of fluid conveying Timoshenko pipeline", *Struct. Eng. Mech.*, **62**(1), 65-77.

Civalek, O. (2004), "Application of differential quadrature (DQ) and harmonic differential quadrature (HDQ) for buckling analysis of thin isotropic plates and elastic columns", *Eng. Struct.*, **26**(2), 171-186.

Cong, P.H. and Duc, N.D. (2018), "New approach to investigate the nonlinear dynamic response and vibration of a functionally graded multilayer graphene nanocomposite plate on a viscoelastic Pasternak medium", *Acta Mech.*, **229**, 3651-3670.

Duc, N.D., Hadavinia, H., Van Thu, P. and Quanm, T.Q. (2015), "Vibration and nonlinear dynamic response of imperfect three-phase polymer nanocomposite panel resting on elastic foundations under hydrodynamic loads", *Compos. Struct.*, **131**, 229-237.

Duc, N.D., Seung-Eock, K., Quan, T.Q., Long, D.D. and Anh, V.M. (2018), "Nonlinear dynamic response and vibration of nanocomposite multilayer organic solar cell", *Compos. Struct.*, **184**, 1137-1144.

Duc, N.D., Tran, Q.Q. and Nguyen, D.K. (2017), "New approach to investigate nonlinear dynamic response and vibration of imperfect functionally graded carbon nanotube reinforced composite double curved shallow shells", *Aerosp. Sci. Technol.*, **71**, 360-372.

García-Macías, E. and Castro-Triguero, R. (2018), "Coupled effect of CNT waviness and agglomeration: A case study of vibrational analysis of CNT/polymer skew plates", *Compos. Struct.*, **193**, 87-102.

Ghaitani, M.M. and Majidian, A. (2017), "Frequency and critical fluid velocity analysis of pipes reinforced with FG-CNTs conveying internal flows", *Wind Struct.*, **24**(3), 267-285.

Ghayesh, M.H. and Farokhi, H. (2018), "On the viscoelastic dynamics of fluid-conveying microtubes", *Int. J. Eng. Sci.*, **127**, 186-200.

Henderson, J.P., Plummer, A. and Johnston, N. (2018), "An electro-hydrostatic actuator for hybrid active-passive vibration isolation", *Int. J. Hydromech.*, **1**(1), 47-71.

Kamarian, S., Salim, M., Dimitri, R. and Tornabene, F. (2016), "Free vibration analysis of conical shells reinforced with agglomerated carbon nanotubes", *Int. J. Mech. Sci.*, **108**, 157-165.

Kamarian, S., Shakeri, M., Yas, M.H., Bodaghi, M. and Pourasghar, A. (2015), "Free vibration analysis of functionally graded nanocomposite sandwich beams resting on Pasternak foundation by considering the agglomeration effect of CNTs", *J. Sandw. Struct. Mater.*, **17**(6), 632-665.

Kiani, K. (2014), "Free vibration of conducting nanoplates exposed to unidirectional in-plane magnetic fields using nonlocal shear deformable plate theories", *Phys. E*, **57**, 179-192.

Lakes, R. (2009), *Viscoelastic Materials*, Cambridge University Press, U.S.A.

Lakis, A.A. and Sinno, M. (1992), "Free vibration of axisymmetric and beam-like cylindrical shells partially filled with liquid", *Int. J. Numer. Meth. Eng.*, **33**(2), 235-268.

Mori, T. and Tanaka, K., (1973), "Average stress in matrix and average elastic energy of materials with Misfitting inclusions", *Acta Metall. Mater.*, **21**(5), 571-574.

Patel, S.N., Datta, P.K. and Sheikh, A.H. (2006), "Buckling and dynamic instability analysis of stiffened shell panels", *Thin-Wall. Struct.*, **44**(3), 321-333.

Qian, S. and Bau, H.H. (2005), "Magneto-hydrodynamic stirrer for stationary and moving fluids", *Sens. Actuat.*, **106**(2), 859-870.

Qian, S. and Bau, H.H. (2009), "Magneto-hydrodynamics based microfluidics", *Mech. Res. Commun.*, **36**(1), 10-21.

Raminnea, M., Biglari, H. and Vakili Tahami, F. (2016), "Nonlinear higher order Reddy theory for temperature-dependent vibration and instability of embedded functionally graded pipes conveying fluid-nanoparticle mixture", *Struct. Eng. Mech.*, **59**(1), 153-186.

Reddy, J.N. (2002), *Mechanics of Laminated Composite Plates and Shells: Theory and Analysis*, 2nd Edition, CRC Press.

Rehab, I. Tian, X., Gu, F. and Andrew Ball, D. (2018), "The influence of rolling bearing clearances on diagnostic signatures based on a numerical simulation and experimental evaluation", *Int. J. Hydromechatron.*, **1**(1), 16-46.

Sanada, K. (2018), "Real-time implementation of Kalman filter for unsteady flow measurement in a pipe", *Int. J. Hydromechatron.*, **1**(1), 3-15.

Shokravi, M. (2017), "Vibration analysis of silica nanoparticles-reinforced concrete beams considering agglomeration effects", *Comput. Concrete*, **19**(3), 333-338.

Shokravi, M. Jalili, N. (2017), "Vibration and stability of embedded cylindrical shell conveying fluid mixed by nanoparticles subjected to harmonic temperature distribution", *Wind Struct.*, **25**(4), 381-395.

Thu, P.V. and Duc, N.D. (2017), "Non-linear dynamic response and vibration of an imperfect three-phase laminated nanocomposite cylindrical panel resting on elastic foundations in thermal environments", *Sci. Eng. Compos. Mater.*, **24**(6), 951-962.

Tohidi, H., Hosseini-Hashemi, S.H., Maghsoudpour, A. and Etemadi, S. (2017), "Strain gradient theory for vibration analysis of embedded CNT-reinforced micro Mindlin cylindrical shells considering agglomeration effects", *Struct. Eng. Mech.*, **62**(5), 551-565.

Tornabene, F., Fantuzzi, N. and Bacciocchi, M. (2017), "Linear static response of nanocomposite plates and shells reinforced by agglomerated carbon nanotubes", *Compos. Part B: Eng.*, **115**, 449-476.

Tornabene, F., Fantuzzi, N., Bacciocchi, M. and Viola, E. (2016), "Effect of agglomeration on the natural frequencies of functionally graded carbon nanotube-reinforced laminated composite doubly-curved shells", *Compos. Part B: Eng.*, **89**, 187-218.

Vakili Tahami, F., Biglari, H. and Raminnea, M. (2017), "Moving load induced dynamic response of functionally graded-carbon nanotubes-reinforced pipes conveying fluid subjected to thermal

load", *Struct. Eng. Mech.*, **64**(4), 515-526.
Wang, L. and Ni, Q. (2009), "A reappraisal of the computational modelling of carbon nanotubes conveying viscous fluid", *Mech. Res. Commun.*, **36**(7), 833-837.
Zamani Nouri, A. (2017), "Mathematical modeling of concrete pipes reinforced with CNTs conveying fluid for vibration and stability analyses", *Comput. Concrete*, **19**(3), 325-331.
Zamani Nouri, A. (2018), "The effect of Fe2O3 nanoparticles instead cement on the stability of fluid-conveying concrete pipes based on exact solution", *Comput. Concrete*, **21**(1), 31-37.

CC

Appendix A

$$N_{xx} = A_{11}\left(\frac{\partial u}{\partial x}+\frac{1}{2}\left(\frac{\partial w}{\partial x}\right)^2\right)+B_{11}\left(\frac{\partial \psi_x}{\partial x}\right) +A_{12}\left(\frac{\partial v}{R\partial\theta}+\frac{w}{R}+\frac{1}{2}\left(\frac{\partial w}{R\partial\theta}\right)^2\right)+B_{12}\left(\frac{\partial \psi_\theta}{R\partial\theta}\right), \tag{A1}$$

$$N_{\theta\theta} = A_{12}\left(\frac{\partial u}{\partial x}+\frac{1}{2}\left(\frac{\partial w}{\partial x}\right)^2\right)+B_{12}\left(\frac{\partial \psi_x}{\partial x}\right) +A_{22}\left(\frac{\partial v}{R\partial\theta}+\frac{w}{R}+\frac{1}{2}\left(\frac{\partial w}{R\partial\theta}\right)^2\right)+B_{22}\left(\frac{\partial \psi_\theta}{R\partial\theta}\right), \tag{A2}$$

$$N_{x\theta} = A_{66}\left(\frac{\partial u}{R\partial\theta}+\frac{\partial v}{\partial x}+\frac{\partial w}{\partial x}\frac{\partial w}{R\partial\theta}\right) +B_{66}\left(\frac{\partial \psi_x}{R\partial\theta}+\frac{\partial \psi_\theta}{\partial x}\right), \tag{A3}$$

$$Q_x = A_{55}\left(\frac{\partial w}{\partial x}+\psi_x\right), \tag{A4}$$

$$Q_x = A_{55}\left(\frac{\partial w}{\partial x}+\psi_x\right), \tag{A5}$$

$$M_{xx} = B_{11}\left(\frac{\partial u}{\partial x}+\frac{1}{2}\left(\frac{\partial w}{\partial x}\right)^2\right)+D_{11}\left(\frac{\partial \psi_x}{\partial x}\right) +B_{12}\left(\frac{\partial v}{R\partial\theta}+\frac{w}{R}+\frac{1}{2}\left(\frac{\partial w}{R\partial\theta}\right)^2\right)+D_{12}\left(\frac{\partial \psi_\theta}{R\partial\theta}\right), \tag{A6}$$

$$M_{\theta\theta} = B_{12}\left(\frac{\partial u}{\partial x}+\frac{1}{2}\left(\frac{\partial w}{\partial x}\right)^2\right)+D_{12}\left(\frac{\partial \psi_x}{\partial x}\right) +B_{22}\left(\frac{\partial v}{R\partial\theta}+\frac{w}{R}+\frac{1}{2}\left(\frac{\partial w}{R\partial\theta}\right)^2\right)+D_{22}\left(\frac{\partial \psi_\theta}{R\partial\theta}\right), \tag{A7}$$

where

$$\left(A_{11},A_{12},A_{22},A_{44},A_{55},A_{66}\right) = \int_{-h/2}^{h/2}\left(1+g\frac{\partial}{\partial t}\right)\left(C_{11},C_{12},C_{22},C_{44},C_{55},C_{66}\right)dz, \tag{A8}$$

$$\left(B_{11},B_{12},B_{22},B_{66}\right) = \int_{-h/2}^{h/2}\left(1+g\frac{\partial}{\partial t}\right)\left(C_{11},C_{12},C_{22},C_{66}\right)z\,dz, \tag{A9}$$

$$\left(D_{11},D_{12},D_{22},D_{66}\right) = \int_{-h/2}^{h/2}\left(1+g\frac{\partial}{\partial t}\right)\left(C_{11},C_{12},C_{22},C_{66}\right)z^2dz, \tag{A10}$$

Appendix B

$$
\begin{aligned}
&A_{11}\left(\frac{\partial^2 u}{\partial x^2}+\frac{\partial w}{\partial x}\frac{\partial^2 w}{\partial x^2}\right)+B_{11}\left(\frac{\partial^2 \psi_x}{\partial x^2}\right)\\
&+A_{12}\left(\frac{\partial^2 v}{R\partial x\,\partial\theta}+\frac{\partial w}{R\partial x}+\frac{\partial w}{R\partial\theta}\frac{\partial^2 w}{R\partial x\,\partial\theta}\right)\\
&+B_{12}\left(\frac{\partial^2 \psi_\theta}{R^2\partial x\,\partial\theta}\right)+\frac{B_{66}}{R}\left(\frac{\partial^2 \psi_x}{R\partial\theta^2}+\frac{\partial^2 \psi_\theta}{\partial x\,\partial\theta}\right)\\
&+\frac{A_{66}}{R}\left(\frac{\partial^2 u}{R\partial\theta^2}+\frac{\partial^2 v}{\partial x\,\partial\theta}+\frac{\partial^2 w}{\partial x\,\partial\theta}\frac{\partial w}{R\partial\theta}+\frac{\partial w}{\partial x}\frac{\partial^2 w}{R\partial\theta^2}\right)\\
&=I_0\frac{\partial^2 u}{\partial t^2}+I_1\frac{\partial^2 \psi_x}{\partial t^2}
\end{aligned}
\tag{B1}
$$

$$
\begin{aligned}
&A_{66}\left(\frac{\partial^2 u}{R\partial\theta\partial x}+\frac{\partial^2 v}{\partial x^2}+\frac{\partial^2 w}{\partial x^2}\frac{\partial w}{R\partial\theta}+\frac{\partial w}{\partial x}\frac{\partial^2 w}{R\partial\theta\partial x}\right)\\
&+B_{66}\left(\frac{\partial^2 \psi_x}{R\partial\theta\partial x}+\frac{\partial^2 \psi_\theta}{\partial x^2}\right)+\frac{A_{12}}{R}\left(\frac{\partial^2 u}{\partial x\,\partial\theta}+\frac{\partial w}{\partial x}\frac{\partial^2 w}{\partial x\,\partial\theta}\right)\\
&+\frac{B_{12}}{R}\left(\frac{\partial^2 \psi_x}{\partial x\,\partial\theta}\right)+\frac{A_{22}}{R}\left(\frac{\partial^2 v}{R\partial\theta^2}+\frac{\partial w}{R\partial\theta}+\frac{\partial w}{R\partial\theta}\frac{\partial^2 w}{R\partial\theta^2}\right)\\
&+\frac{B_{22}}{R}\left(\frac{\partial^2 \psi_\theta}{R^2\partial\theta^2}\right)=I_0\frac{\partial^2 v}{\partial t^2}
\end{aligned}
\tag{B2}
$$

$$
\begin{aligned}
&A_{55}\left(\frac{\partial^2 w}{\partial x^2}+\frac{\partial \psi_x}{\partial x}\right)+\frac{A_{44}}{R}\left(\frac{\partial^2 w}{R\partial\theta^2}-\frac{\partial v}{R\partial\theta}+\frac{\partial \psi_\theta}{\partial\theta}\right)\\
&+\mu_f\frac{\partial^2}{\partial x^2}\left(\frac{\partial w}{\partial t}+v_x\frac{\partial w}{\partial x}\right)+\sigma H_x^2\left(\frac{\partial w}{\partial t}+v_x\frac{\partial w}{\partial x}\right)\\
&-\rho_f\left(\frac{\partial}{\partial t}+V_f\frac{\partial}{\partial x}\right)\left(\frac{\partial w}{\partial t}+v_x\frac{\partial w}{\partial x}\right)\\
&+\eta h H_x^2\left(\frac{\partial^2 w}{\partial x^2}-\frac{\partial^2 w}{R^2\partial\theta^2}\right)=I_0\frac{\partial^2 w}{\partial t^2},
\end{aligned}
\tag{B3}
$$

$$
\begin{aligned}
&B_{11}\left(\frac{\partial^2 u}{\partial x^2}+\frac{\partial w}{\partial x}\frac{\partial^2 w}{\partial x^2}\right)+D_{11}\left(\frac{\partial^2 \psi_x}{\partial x^2}\right)\\
&+B_{12}\left(\frac{\partial^2 v}{R\partial\theta\partial x}+\frac{\partial w}{\partial x}+\frac{\partial^2 w}{R\partial\theta\partial x}\right)+D_{12}\left(\frac{\partial^2 \psi_\theta}{R\partial\theta\partial x}\right)\\
&+\frac{B_{66}}{R}\left(\frac{\partial^3 u}{R\partial x\,\partial\theta^2}+\frac{\partial^2 v}{\partial x\,\partial\theta}+\frac{\partial^2 w}{\partial x\,\partial\theta}\frac{\partial w}{R\partial\theta}+\frac{\partial w}{\partial x}\frac{\partial^2 w}{R\partial\theta^2}\right)\\
&+\frac{D_{66}}{R}\left(\frac{\partial^2 \psi_x}{R\partial\theta^2}+\frac{\partial^2 \psi_\theta}{\partial x\,\partial\theta}\right)-A_{55}\left(\frac{\partial w}{\partial x}+\psi_x\right)\\
&=I_1\frac{\partial^2 u}{\partial t^2}+I_2\frac{\partial^2 \psi_x}{\partial t^2}
\end{aligned}
\tag{B4}
$$

$$
\begin{aligned}
&B_{66}\left(\frac{\partial^2 u}{R\partial\theta\partial x}+\frac{\partial^2 v}{\partial x^2}+\frac{\partial^2 w}{\partial x^2}\frac{\partial w}{R\partial\theta}+\frac{\partial w}{\partial x}\frac{\partial^2 w}{R\partial\theta\partial x}\right)\\
&+D_{66}\left(\frac{\partial^2 \psi_x}{R\partial\theta\partial x}+\frac{\partial^2 \psi_\theta}{\partial x^2}\right)+\frac{B_{12}}{R}\left(\frac{\partial^2 u}{\partial x\,\partial\theta}+\frac{\partial w}{\partial x}\frac{\partial^2 w}{\partial x\,\partial\theta}\right)\\
&+\frac{D_{12}}{R}\left(\frac{\partial^2 \psi_x}{\partial x\,\partial\theta}\right)+\frac{B_{22}}{R}\left(\frac{\partial^2 v}{R\partial\theta^2}+\frac{\partial w}{R\partial\theta}+\frac{\partial w}{R\partial\theta}\frac{\partial^2 w}{R\partial\theta^2}\right)\\
&+\frac{D_{22}}{R}\left(\frac{\partial^2 \psi_\theta}{R\partial\theta^2}\right)-A_{44}\left(\frac{\partial w}{R\partial\theta}-\frac{v}{R}+\psi_\theta\right)\\
&=I_1\frac{\partial^2 v}{\partial t^2}+I_2\frac{\partial^2 \psi_\theta}{\partial t^2}
\end{aligned}
\tag{B5}
$$